PLOS | ONE

RESEARCH ARTICLE

Radiative Peristaltic Flow of Jeffrey Nanofluid with Slip Conditions and Joule Heating

Tasawar Hayat[1,2], Maryam Shafique[1], Anum Tanveer[1]*, Ahmed Alsaedi[2]

1 Department of Mathematics, Quaid-I-Azam University 45320, Islamabad 44000, Pakistan, **2** NAAM Research Group, Department of Mathematics, Faculty of Science, King Abdulaziz University, Jeddah 21589, Saudi Arabia

* anum@math.qau.edu.pk

Abstract

Mixed convection peristaltic flow of Jeffrey nanofluid in a channel with compliant walls is addressed here. The present investigation includes the viscous dissipation, thermal radiation and Joule heating. Whole analysis is performed for velocity, thermal and concentration slip conditions. Related problems through long wavelength and low Reynolds number are examined for stream function, temperature and concentration. Impacts of thermal radiation, Hartman number, Brownian motion parameter, thermophoresis, Joule heating and slip parameters are explored in detail. Clearly temperature is a decreasing function of Hartman number and radiation parameter.

Citation: Hayat T, Shafique M, Tanveer A, Alsaedi A (2016) Radiative Peristaltic Flow of Jeffrey Nanofluid with Slip Conditions and Joule Heating. PLoS ONE 11(2): e0148002. doi:10.1371/journal.pone.0148002

Editor: Bing-Yang Cao, Tsinghua University, CHINA

Received: December 2, 2015

Accepted: January 11, 2016

Published: February 17, 2016

Data Availability Statement: All relevant data are within the paper and its reference list.

Funding: The authors have no support or funding to report.

Competing Interests: The authors have declared that no competing interests exist.

1 Introduction

Peristaltic activity has great value in many physiological processes and industries. Peristalsis can occur due to contraction and expansion of flexible boundaries. In other words this activity includes passing down, mixing and transporting materials through contraction or expansion of the waves propagating along the channel walls. It has wide applications in medical industry and chemical processes. Typical examples in this direction include in distillation towers and fixed-bed reactors, urine transport from kidney to bladder through the ureter, transport of lymph in the lymphatic vessels, swallowing food through the esophagus, the movement of chyme in the gastrointestinal tract, ovum movement in the fallopian tube, transport of corrosive fluids, sanitary fluid transport and blood pumps in heart lung machine etc. The worms utilize peristalsis for locomotion. Latham [1] and Shapiro et al. [2] initiated works on peristalsis of viscous fluids via theoretical and experimental approaches. Later on many researchers put forward their research on this topic by considering different kinds of fluid models, no-slip/ partial slip condition and one or more assumptions of long wavelength, low Reynolds number, small amplitude ratio, small wave number etc. Especially the magnetohydrodynamics (MHD) peristaltic transport of fluid in a channel are quite important with reference to conductive physiological materials for example the blood, blood pump machines and with the need of both experimental and theoretical research for operation of peristaltic MHD compressor. Concept of magnetohydrodynamics is useful in Magnetic Resonance Imaging (MRI) when a patient

undergoes in a height static magnetic field. On the other hand the heat transfer in peristalsis is useful in the oxygenation processes. Such concept in further important in the industrial applications like sanitary fluid transport and transport of corrosive materials where the fluid contact with the machinery parts is prohibited. Note that the heat transfer on skin surface occurs by any of the four processes namely evaporation, convection, conduction and radiation. Having all such aspects in mind many authors in past analyzed the peristaltic flows in detail (see [3–16]). Nadeem and Akbar [17] studied influence of radially varying MHD on the peristaltic flow in an annulus. Ellahi and Hussain [18] analyzed effects of MHD and partial slip on peristaltic flow of Jeffrey fluid in a rectangular duct. Ali et al. [19] analyzed numerical simulation of peristaltic flow of a biorheological fluid with shear dependent viscosity in a curved channel.

Mixed convection occurs in vertical channels for improvement of cooling systems in engineering. Analysis of heat transfer with MHD and mixed convection in vertical channels has great applications in solar energy collection, chemical reactions and cooling systems. Sheikholeslami et al. [20] analyzed simulation of MHD CuO–water nanofluid flow and convective heat transfer using Lorentz forces. Abbasi et al. [21] discussed effects of inclined magnetic field and Joule heating in mixed convective flows of non-Newtonian fluids. Mustafa et al. [22] analyzed Soret and Dufour effects in the mixed convective peristaltic flow of fourth grade fluid. Soret and Dufour effects in mixed convective peristalsis of viscous nanofluids are examined by Hayat et al. [23]. Srinivas and Muthuraj [24] addressed mixed convective peristalsis in presence of chemical reaction. Heat and mass transfer analysis in mixed convective peristaltic transport of viscous fluid in an asymmetric channel is studied by Srinivas et al. [25]. It has been noticed that not much information is available for mixed convective peristalsis of non-Newtonian fluid in a channel especially with compliant walls and nanoparticles. The purpose here is to examine the mixed convective peristaltic flow of Jeffrey nanofluid in a compliant walls channel. In addition thermal radiation effect is considered. The channel walls exhibit velocity, thermal and concentration slip conditions. Joule heating is taken into account. Results for velocity, temperature and concentration are obtained.

Peristaltic transport has not been conducted well in connection with elastic behavior of the walls. Wall properties such as elastic tension and damping are of immense importance in practical circumstances. Graphical results are plotted to analyze the behavior of sundry parameters on temperature, velocity, nanoparticle concentration and heat transfer coefficient.

2 Modeling

We consider two-dimensional flow of an incompressible Jeffrey nanofluid in a symmetric channel of uniform thickness $2d_1$. The sinusoidal wave is propagating along the walls of the channel with wavelength λ and constant speed c. The axial and transverse directions are indicated by x and y respectively. Let $y = -\eta$ and $y = +\eta$ shows the left and right positions of the channel boundaries (see Fig 1). A magnetic field of strength B_0 is applied. The effects of induced magnetic field is negligible for small magnetic Reynolds number. The slip conditions for velocity, temperature and concentration are considered. The electric field is considered absent. The walls of channel are taken flexible. The wall geometry can be described by the expression

$$y = \pm\eta(x,t) = \pm\left[d_1 + a\sin\frac{2\pi}{\lambda}(x - ct)\right], \tag{1}$$

where c is the wave speed, a the wave amplitude, λ the wavelength, $2d_1$ the width of channel

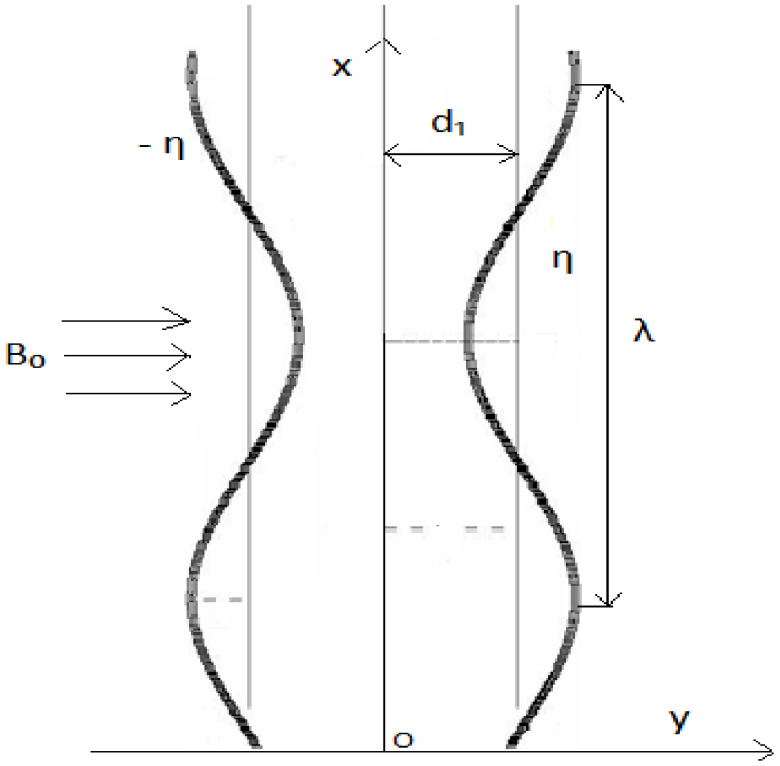

Fig 1. Geometry of the problem.

doi:10.1371/journal.pone.0148002.g001

and t the time. Expression of Cauchy stress tensor (τ) for Jeffrey material is

$$\tau = -p\mathbf{I} + \mathbf{S},$$

$$\mathbf{S} = \frac{\mu}{1+\lambda_1}\left(\dot{\gamma} + \lambda_2 \frac{d\dot{\gamma}}{dt}\right).$$

Here $\mathbf{S}$ represent extra stress tensor, λ_1 shows the ratio of relaxation to retardation times, λ_2 the retardation time, p the pressure, I the identity tensor, μ the coefficient of viscosity, $\dot{\gamma}$ the shear rate, $\frac{d}{dt}$ the material time differentiation and (u, v) are the components of velocity. The equations governing the flow are given by

$$\frac{\partial u}{\partial x} + \frac{\partial v}{\partial y} = 0, \tag{2}$$

$$\begin{aligned}\frac{\partial u}{\partial t} + u\frac{\partial u}{\partial x} + v\frac{\partial u}{\partial y} = & -\frac{1}{\rho_f}\frac{\partial p}{\partial x} + \frac{1}{\rho_f}\frac{\partial S_{xx}}{\partial x} + \frac{1}{\rho_f}\frac{\partial S_{xy}}{\partial y} - \frac{\sigma B_0^2 u}{\rho_f} + (1 - C_0)g\alpha(T - T_0) \\ & + \left(\frac{\rho_p - \rho_f}{\rho_f}\right)g\beta(C - C_0),\end{aligned} \tag{3}$$

$$\frac{\partial v}{\partial t} + u\frac{\partial v}{\partial x} + v\frac{\partial v}{\partial y} = -\frac{1}{\rho_f}\frac{\partial p}{\partial y} + \frac{1}{\rho_f}\frac{\partial S_{xy}}{\partial x} + \frac{1}{\rho_f}\frac{\partial S_{yy}}{\partial y}, \tag{4}$$

$$\begin{aligned}\frac{\partial T}{\partial t}+u\frac{\partial T}{\partial x}+v\frac{\partial T}{\partial y} &= \alpha\left(\frac{\partial^2 T}{\partial x^2}+\frac{\partial^2 T}{\partial y^2}\right)+\frac{1}{\rho_f c_f}\left[S_{xx}\frac{\partial u}{\partial X}+S_{xy}\left(\frac{\partial u}{\partial y}+\frac{\partial v}{\partial x}\right)+S_{yy}\frac{\partial v}{\partial y}\right]\\ &+\frac{1}{\rho_f c_f}\left(\frac{\partial q_r}{\partial y}+\frac{\partial q_r}{\partial x}\right)+\frac{\sigma B_0^2 u^2}{\rho_f c_f}\\ &+\tau\left[D_B\left(\frac{\partial C}{\partial x}\frac{dT}{dx}+\frac{\partial C}{\partial y}\frac{dT}{dy}\right)+\frac{D_T}{T_m}\left\{\left(\frac{\partial T}{\partial x}\right)^2+\left(\frac{\partial T}{\partial y}\right)^2\right\}\right],\end{aligned} \tag{5}$$

$$\frac{\partial C}{\partial t}+u\frac{\partial C}{\partial x}+v\frac{\partial C}{\partial y}=D_B\left(\frac{\partial^2 C}{\partial x^2}+\frac{\partial^2 C}{\partial y^2}\right)+\frac{D_T}{T_m}\left(\frac{\partial^2 T}{\partial x^2}+\frac{\partial^2 T}{\partial y^2}\right), \tag{6}$$

Radiative heat flux q_r is given by

$$q_r=-\frac{4\sigma^*}{3k^*}\frac{\partial T^4}{\partial y}, \tag{7}$$

where σ^* is the Stefan–Boltzmann constant having numerical value $1.380648\times10^{-23}JK^{-1}$ and k^* is the mean absorption coefficient. We assume that the temperature difference within the flow is sufficiently small. Hence expanding T^4about T_0 and neglecting higher order terms one obtains

$$T^4\cong 4T_0^3T-3T_0^4.$$

The above expression and Eq (7) now yield

$$q_r=\frac{-16\sigma^*T_0^3}{3k^*}\frac{\partial T}{\partial y}. \tag{8}$$

The relevant boundary conditions are

$$u\pm\beta_1\frac{\mu}{1+\lambda_1}\left(1+\lambda_2\left(u\frac{\partial}{\partial x}+v\frac{\partial}{\partial y}\right)\right)\left(\frac{\partial u}{\partial y}+\frac{\partial v}{\partial x}\right)=0,\quad at\quad y=\pm\eta, \tag{9}$$

$$T\pm\beta_2\frac{\partial T}{\partial y}=\begin{pmatrix}T_1\\T_0\end{pmatrix},\quad C\pm\beta_3\frac{\partial C}{\partial y}=\begin{pmatrix}C_1\\C_0\end{pmatrix},\quad at\quad y=\pm\eta, \tag{10}$$

$$\begin{aligned}\left[-\tau_1\frac{\partial^3}{\partial x^3}+m_1\frac{\partial^3}{\partial x\partial t^2}+d\frac{\partial^2}{\partial x\partial t}\right]\eta &= \frac{\partial S_{xx}}{\partial x}+\frac{\partial S_{xy}}{\partial y}-\rho_f\left(\frac{\partial u}{\partial t}+u\frac{\partial u}{\partial x}+v\frac{\partial u}{\partial y}\right)-\sigma B_0^2u\\ &-(1-C_0)\rho_f g\alpha(T-T_0)+(\rho_p-\rho_f)g\beta(C-C_0),\ \text{at}\ \ y=\pm\eta.\end{aligned} \tag{11}$$

In the above equations ρ_f is the density of the nanofluid, ν the kinematic viscosity, α the thermal diffusivity, σ the thermal conductivity, S_{xx}, S_{xy}, S_{yy} the components of extra stress tensor, D_B the Brownian motion coefficient, D_T the thermophoretic diffusion coefficient and $\tau^*=\frac{(\rho c)_p}{(\rho c)_f}$ the ratio of effective heat capacity of nanoparticle material to heat capacity of fluid, τ_1 the elastic tension, m_1 the mass per unit area, d_1 the coefficient of viscous damping, $\beta_1, \beta_2, \beta_3$ the velocity, thermal and concentration slip parameters respectively, T_m the mean temperature, T_1 and C_1 the temperature and the concentration at the right wall respectively while T_0 and C_0 the temperature and the concentration at the left wall respectively.

Introducing the following non-dimensional quantities:

$$\begin{aligned} u^* &= \frac{u}{c},\ v^* = \frac{v}{c},\ x^* = \frac{x}{\lambda},\ y^* = \frac{y}{d_1},\ \beta_i^* = \frac{\beta_i}{d_1}(i=1,2,3),\ t^* = \frac{ct}{\lambda},\ \eta^* = \frac{\eta}{d_1},\ p^* = \frac{d_1^2 p}{c\lambda\mu},\ K = \frac{k}{d^2}, \\ \theta &= \frac{T-T_0}{T_1-T_0},\ \phi = \frac{C-C_0}{C_1-C_0},\ Gr = \frac{(1-C_0)\rho_f g\alpha d^2(T_1-T_0)}{c\mu},\ Qr = \frac{\left(\rho_c-\rho_f\right)g\beta d^2(C_1-C_0)}{c\mu}, \\ E_1 &= -\frac{\tau d_1^3}{\lambda^3\mu c},\ E_2 = \frac{m_1 d_1^3 c}{\lambda^3\mu},\ E_3 = \frac{d d_1^3}{\lambda^2\mu},\ Rn = \frac{16\sigma T_0^3}{3k\mu c_f},\ s_{ij} = \frac{d_1}{\mu c}S_{ij}^*,\ \lambda_2^* = \frac{\lambda_2 c}{d_1}. \end{aligned} \tag{12}$$

Eqs (3)–(6) after omitting asterisks and writing stream function $\psi(x, y, t)$ by the definition [7]:

$$u = \frac{\partial\psi}{\partial y}, \qquad v = -\delta\frac{\partial\psi}{\partial x},$$

become

$$\begin{aligned} Re\left[\delta\frac{\partial^2\psi}{\partial t\partial y} + \delta\frac{\partial\psi}{\partial y}\frac{\partial^2\psi}{\partial x\partial y} - \delta\frac{\partial\psi}{\partial x}\frac{\partial^2\psi}{\partial y^2}\right] &= -\frac{\partial p}{\partial x} + \delta\frac{\partial s_{xx}}{\partial x} + \frac{\partial s_{xy}}{\partial y} \\ &\quad + Gr\theta + Qr\phi - M^2 u, \end{aligned} \tag{13}$$

$$Re\ \delta\left[-\delta^2\frac{\partial^2\psi}{\partial x\partial t} - \delta^2\frac{\partial\psi}{\partial y}\frac{\partial^2\psi}{\partial x^2} - \delta^2\frac{\partial^2\psi}{\partial x\partial y}\right] = -\frac{\partial p}{\partial y} + \delta^2\frac{\partial s_{xy}}{\partial x} + \delta\frac{\partial s_{yy}}{\partial y}, \tag{14}$$

$$\begin{aligned} Re\left[\delta\frac{\partial\theta}{\partial t} + u\delta\frac{\partial\theta}{\partial x} + v\frac{\partial\theta}{\partial y}\right] &= Ec\left(\frac{1}{1+\lambda_1}\right)\left[\left(1+\lambda_2^*\delta\left(\frac{\partial\psi}{\partial y}\frac{\partial}{\partial x} - \frac{\partial\psi}{\partial x}\frac{\partial}{\partial y}\right)\right)\left(4\delta^2\left(\frac{\partial^2\psi}{\partial x\partial y}\right)^2 + \left(-\delta^2\frac{\partial^2\psi}{\partial x^2} + \frac{\partial^2\psi}{\partial y^2}\right)^2\right)\right] \\ &\quad + Rn\left(\delta\frac{\partial^2\theta}{\partial x\partial y} + \frac{\partial^2\theta}{\partial y^2}\right) + \frac{1}{\mathrm{Pr}}\left(\delta^2\frac{\partial^2\theta}{\partial x^2} + \frac{\partial^2\theta}{\partial y^2}\right) + EcM^2\left(\frac{\partial\psi}{\partial y}\right)^2 \\ &\quad + Nb\left[\delta^2\frac{\partial\phi}{\partial x}\frac{\partial\theta}{\partial x} + \frac{\partial\phi}{\partial y}\frac{\partial\theta}{\partial y}\right] + Nt\left[\left(\delta\frac{\partial\theta}{\partial x}\right)^2 + \left(\frac{\partial\theta}{\partial y}\right)^2\right], \end{aligned} \tag{15}$$

$$Re\,Sc\left[\delta\frac{\partial\phi}{\partial t} + \delta\frac{\partial\psi}{\partial y}\frac{\partial\phi}{\partial x} - \delta\frac{\partial\psi}{\partial x}\frac{\partial\phi}{\partial y}\right] = \left(\delta^2\frac{\partial^2\phi}{\partial x^2} + \frac{\partial^2\phi}{\partial y^2}\right) + \frac{Nt}{Nb}\left(\delta^2\frac{\partial^2\theta}{\partial x^2} + \frac{\partial^2\theta}{\partial y^2}\right), \tag{16}$$

with the boundary conditions

$$\frac{\partial\psi}{\partial y} \pm \beta_1\frac{1}{1+\lambda_1}\left[1+\lambda_2^*\delta\left(\frac{\partial\psi}{\partial y}\frac{\partial}{\partial x} - \delta^2\frac{\partial\psi}{\partial x}\frac{\partial}{\partial y}\right)\right]\left(\frac{\partial^2\psi}{\partial y^2} - \delta\frac{\partial^2\psi}{\partial x^2}\right) = 0, \quad at \quad y = \pm\eta, \tag{17}$$

$$\theta \pm \beta_2\frac{\partial\theta}{\partial y} = \begin{pmatrix}1\\0\end{pmatrix}, \quad \phi \pm \beta_3\frac{\partial\phi}{\partial y} = \begin{pmatrix}1\\0\end{pmatrix}, \quad at \quad y = \pm\eta, \tag{18}$$

$$\left[E_1\frac{\partial^3}{\partial x^3} + E_2\frac{\partial^3}{\partial x\partial t^2} + E_3\frac{\partial^2}{\partial x\partial t}\right]\eta = \frac{1}{1+\lambda_1}(1+\delta\frac{\partial\psi}{\partial y}\frac{\partial}{\partial x})\frac{\partial^3\psi}{\partial y^3} + Gr\theta + Qr\phi - M^2\frac{\partial\psi}{\partial y}, \quad at \quad y = \pm\eta, \tag{19}$$

where

$$s_{xx}=\frac{2\delta}{1+\lambda_1}\left[1+\lambda_2^*\delta\left(\frac{\partial\psi}{\partial y}\frac{\partial}{\partial x}-\frac{\partial\psi}{\partial x}\frac{\partial}{\partial y}\right)\right]\frac{\partial^2\psi}{\partial x\partial y},$$
$$s_{xy}=\frac{1}{1+\lambda_1}\left[1+\lambda_2^*\delta\left(\frac{\partial\psi}{\partial y}\frac{\partial}{\partial x}-\frac{\partial\psi}{\partial x}\frac{\partial}{\partial y}\right)\right]\left(\frac{\partial^2\psi}{\partial y^2}-\delta^2\frac{\partial^2\psi}{\partial x^2}\right),$$
$$s_{yy}=-\frac{2\delta}{1+\lambda_1}\left[1+\lambda_2^*\delta\left(\frac{\partial\psi}{\partial y}\frac{\partial}{\partial x}-\frac{\partial\psi}{\partial x}\frac{\partial}{\partial y}\right)\right]\frac{\partial^2\psi}{\partial x\partial y},$$

After employing long wavelength and low Reynolds number approximations [18] one has the following problems

$$\left(\frac{1}{1+\lambda_1}\right)\frac{\partial^4\psi}{\partial y^4}+Gr\frac{\partial\theta}{\partial y}+Qr\frac{\partial\phi}{\partial y}-M^2\frac{\partial^2\psi}{\partial y^2}=0, \tag{20}$$

$$\begin{aligned}&(1+Rn\,\mathrm{Pr})\frac{\partial^2\theta}{\partial y^2}+Nb\,\mathrm{Pr}\frac{\partial\theta}{\partial y}\frac{\partial\phi}{\partial y}+Nt\,\mathrm{Pr}\left(\frac{\partial\theta}{\partial y}\right)^2\\&+Br\quad\left[\frac{1}{1+\lambda_1}\left(\frac{\partial^2\psi}{\partial y^2}\right)^2+M^2\left(\frac{\partial\psi}{\partial y}\right)^2\right]=0,\end{aligned} \tag{21}$$

$$\frac{\partial^2\phi}{\partial y^2}+\frac{Nt}{Nb}\left(\frac{\partial^2\theta}{\partial y^2}\right)=0, \tag{22}$$

$$\frac{\partial\psi}{\partial y}\pm\beta_1\left(\frac{1}{1+\lambda_1}\right)\left(\frac{\partial^2\psi}{\partial y^2}\right)=0,\theta\pm\beta_2\frac{\partial\theta}{\partial y}=\binom{1}{0},\phi\pm\beta_3\frac{\partial\phi}{\partial y}=\binom{1}{0},\quad at\quad y=\pm\eta, \tag{23}$$

$$\left[E_1\frac{\partial^3}{\partial x^3}+E_2\frac{\partial^3}{\partial x\partial t^2}+E_3\frac{\partial^2}{\partial x\partial t}\right]\eta=\left(\frac{1}{1+\lambda_1}\right)\frac{\partial^3\psi}{\partial y^3}+Gr\theta+Qr\phi-M^2\frac{\partial\psi}{\partial y},\quad at\quad y=\pm\eta, \tag{24}$$

where $\epsilon=\frac{a}{d_1}$ represents the amplitude ratio, $\delta=\frac{d_1}{\lambda}$ the wave number, $Nb=\frac{\tau^*D_B(C_1-C_0)}{\nu}$ and $Nt=\frac{\tau^*D_T(T_1-T_0)}{T_m\nu}$ the Brownian motion and thermophoresis parameters respectively, $Re=\frac{c\rho d_1}{\mu}$ the Reynolds number, $Sc=\frac{\nu}{D_B}$ the Schmidt number, $M=\sqrt{\frac{\pi}{\mu}}B_0d_1$ the Hartman number, $Ec=\frac{c^2}{c_f(T_1-T_0)}$ the Eckert number, $\mathrm{Pr}=\frac{\nu\rho c_p}{k}$ the Prandtl number, Qr the local nanoparticle Grashoff number and Br = PrEc the Brinkman number, Pr the Prandtl number and Ec Eckert number. Heat transfer coefficient in non-dimensional form is given by

$$Z=\eta_x\frac{\partial\theta}{\partial y}\bigg|_{y=\eta}. \tag{25}$$

3 Discussion

The purpose of this portion is to predict the behaviors of velocity, temperature, nanoparticle concentration and heat transfer rate under the impact of emerging parameters. Hence the graphical results are obtained numerically through NDSolve in Mathematica. The relevant physical explanations are presented in this section.

3.1 Velocity profile

Fig 2 represents the impact of various parameters on velocity. In (Fig 2(a)) it is observed that for larger velocity slip parameter β_1, the velocity increases. As fluid slip is the deviation in the angle at which the fluid leaves the channel. Therefore an increase in β_1 causes non-uniform velocity distribution inside the channel (see Fig 2(a)). The effect is useful in determining the accurate estimation of energy transfer between the channel and the fluid. Similar result has been obtained by Hayat et. al [13] in their study for nanofluids. The reason behind the increasing behavior of β_1 is that the resistance is reduced due to slip hence velocity increases. Increasing Grashoff number Gr decreases drag forces and hence velocity profile increases (see Fig 2 (b)). It is seen that velocity is an increasing function of Jeffrey fluid parameter λ_1 and local nanoparticle Grashoff number Qr (see Fig 2(c) and 2(d)). Magnetic field applied in transverse direction acts as a retarding force for the fluid flow and thus the velocity profile decreases for increasing values of Hartman number M (see Fig 2(e)). Due to elasticity of flexible walls the velocity profile shows increasing behavior for larger E_1 and E_2 while velocity profile decreases upon enhancement in E_3 due to its viscous damping effect (see Fig 2(f)). For reliability the results obtained for wall parameters can be compared with the previous analysis of Hina et al. [11] for curved channel and Hayat et al. [13] for planer channel.

3.2 Temperature profile

Fig 3 displays the impacts of various parameters on temperature profile. It is observed from Fig 3(a) that temperature profile increases for larger thermal slip parameter β_2. Fig 3(b) is plotted to see the variation of Brinkman number Br on temperature. Brinkman number arises due to

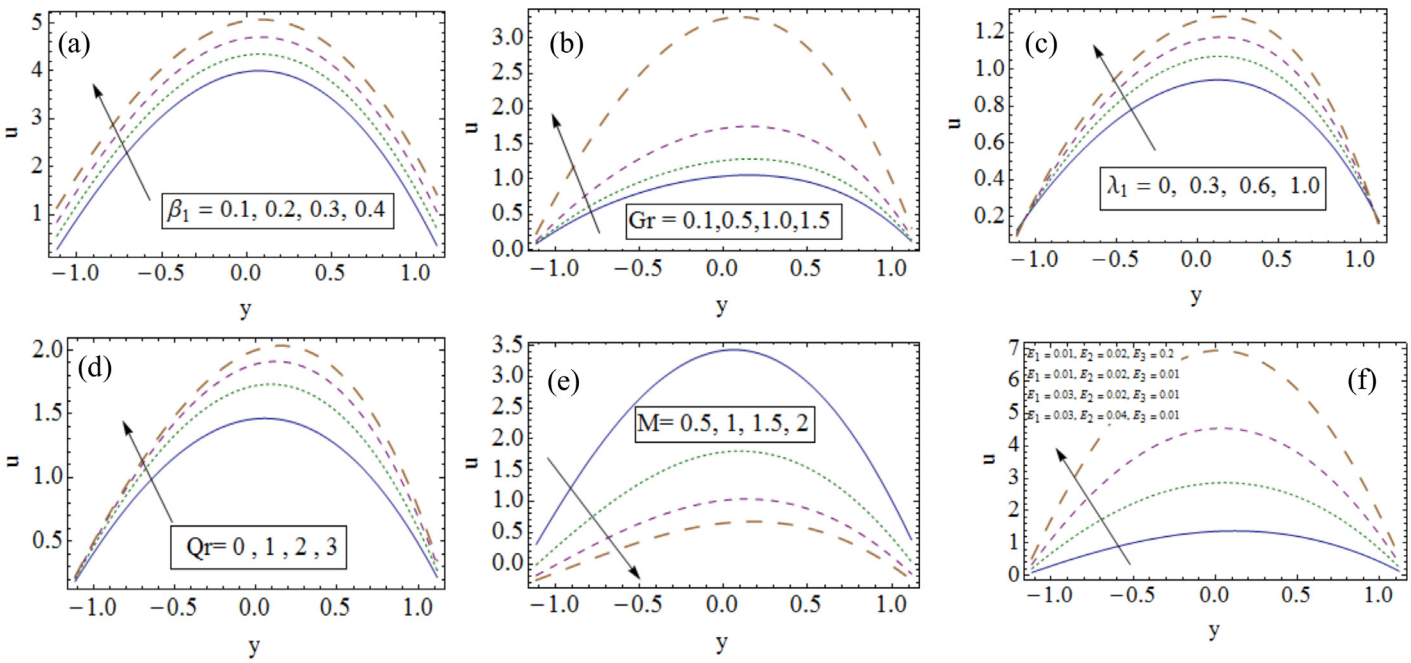

Fig 2. Influences of different parameters on velocity when (a). $x = 0.2$, $t = 0.1$, Pr = 1.5, $Nt = 0.1$, $Nb = 0.1$, $Br = 1.7$, $Qr = 1$, $Gr = 1.5$, $\epsilon = 0.2$, $M = 0.2$, $E_1 = 0.01$, $E_2 = 0.02$, $E_3 = 0.01$, $\beta_2 = 0.1$, $\beta_3 = 0.1$, $\lambda_1 = 1$, $Rn = 1$. (b). $x = 0.2$, $t = 0.1$, Pr = 0.8, $Nt = 0.3$, $Nb = 0.2$, $Br = 1.7$, $Qr = 1$, $\epsilon = 0.2$, $M = 1$, $E_1 = 0.01$, $E_2 = 0.02$, $E_3 = 0.01$, $\beta_1 = 0.1$, $\beta_2 = 0.1$, $\beta_3 = 0.1$, $\lambda_1 = 1$, $Rn = 1$. (c). $x = 0.2$, $t = 0.1$, Pr = 0.8, $Nt = 0.3$, $Nb = 0.2$, $Nt = 1.7$, $Qr = 1$, $Gr = 0.5$, $\epsilon = 0.2$, $M = 1$, $E_1 = 0.01$, $E_2 = 0.02$, $E_3 = 0.01$, $\beta_1 = 0.1$, $\beta_2 = 0.1$, $\beta_3 = 0.1$, $Rn = 1$. (d). $x = 0.2$, $t = 0.1$, $Pr = 1$, $Nt = 0.1$, $Nb = 0.1$, $Br = 1.7$, $Gr = 1.5$, $\epsilon = 0.2$, $M = 0.2$, $E_1 = 0.01$, $E_2 = 0.02$, $E_3 = 0.01$, $\beta_1 = 0.1$, $\beta_2 = 0.1$, $\beta_3 = 0.1$, $\lambda_1 = 0.1$, $Rn = 1$. (e). $x = 0.2$, $t = 0.1$, $Pr = 1$, $Nt = 0.1$, $Nb = 0.1$, $Br = 0.5$, $Qr = 0.3$, $Gr = 1$, $\epsilon = 0.2$, $M = 0.2$, $\beta_1 = 0.1$, $\beta_2 = 0.1$, $\beta_3 = 0.1$, $\lambda_1 = 1$, $Rn = 1$. (f). $x = 0.2$, $t = 0.1$, Pr = 1.5, $Nt = 0.1$, $Nb = 0.1$, $Br = 1.7$, $Qr = 1$, $Gr = 1.5$, $\epsilon = 0.2$, $M = 0.2$, $\beta_1 = 0.1$, $\beta_2 = 0.1$, $\beta_3 = 0.1$, $\lambda_1 = 1$, $Rn = 1$.

doi:10.1371/journal.pone.0148002.g002

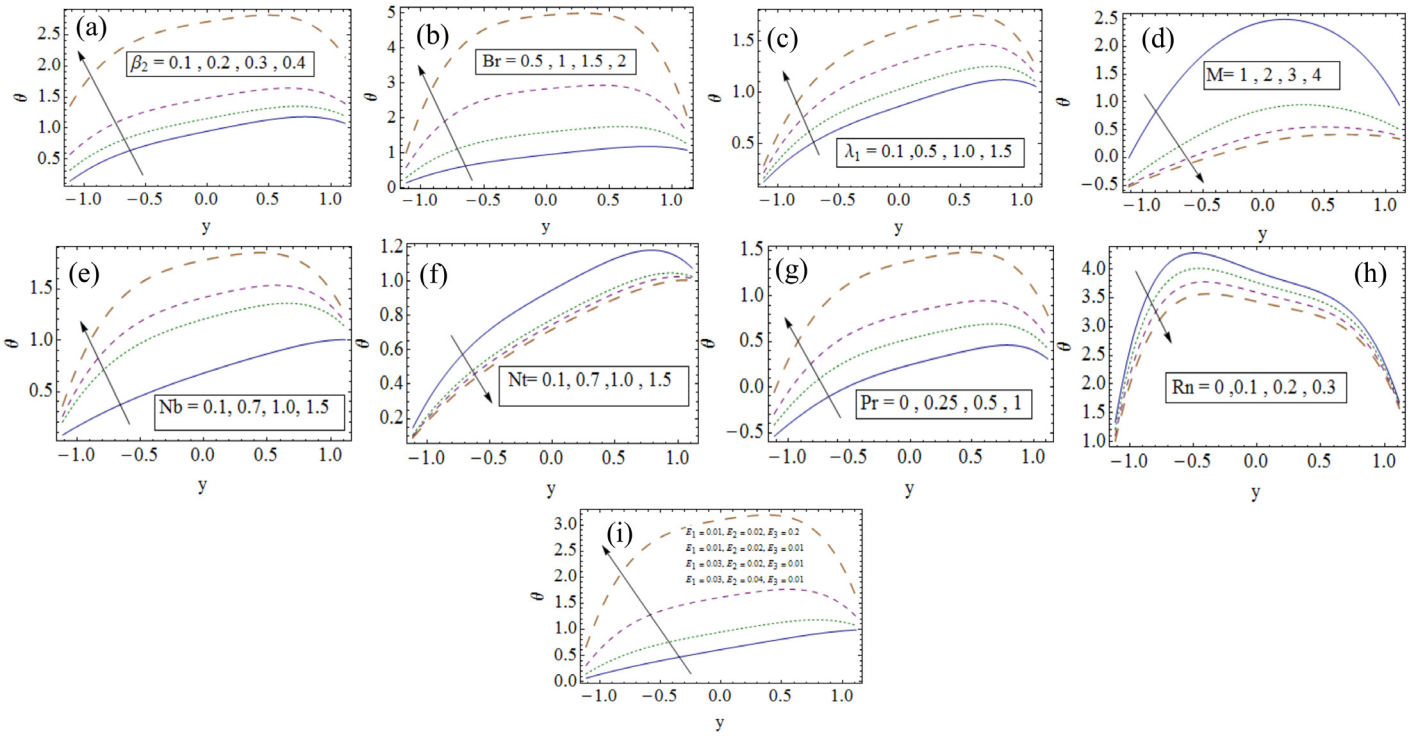

Fig 3. Influences of different parameters on temperature profile when (a). $x = \epsilon = 0.2$, $t = 0.1$, $Rn = 1$, $Gr = 1$, $Qr = 0.3$, $\lambda_1 = 1$, $Br = 0.5$, $Pr = 1$, $Nt = Nb = 0.1$, $M = 0.2$, $\beta_1 = \beta_3 = 0.1$, $E_1 = E_3 = 0.01$, $E_2 = 0.02$. (b). $x = \epsilon = 0.2$, $t = 0.1$, $\lambda_1 = 0.3$, $Rn = 1$, $Gr = 1.5$, $Qr = 1$, $Pr = 1$, $Nt = Nb = 0.1$, $M = 0.2$, $\beta_1 = \beta_2 = \beta_3 = 0.1$, $E_1 = E_3 = 0.01$, $E_2 = 0.02$. (c). $x = \epsilon = 0.2$, $t = 0.1$, $Rn = 1$, $Gr = 1.5$, $Qr = 1$, $Br = 0.5$, $Pr = 1$, $Nt = Nb = 0.1$, $M = 0.2$, $\beta_1 = \beta_2 = \beta_3 = 0.1$, $E_1 = E_3 = 0.01$, $E_2 = 0.02$. (d). $x = \epsilon = 0.2$, $t = 0.1$, $Gr = 1$, $Qr = 1$, $Rn = 1$, $Gr = 1.5$, $Qr = 1$, $\lambda_1 = 0.3$, $Br = 0.5$, $Pr = 1$, $Nt = Nb = 0.1$, $M = 0.2$, $\beta_1 = \beta_3 = 0.1$, $E_1 = E_3 = 0.01$, $E_2 = 0.02$. (e). $x = \epsilon = 0.2$, $t = 0.1$, $Rn = 1$, $Gr = 1.5$, $Qr = 0.3$, $\lambda_1 = 1$, $Br = 0.5$, $Pr = 1$, $Nt = 0.1$, $M = 0.5$, $\beta_1 = \beta_2 = \beta_3 = 0.1$, $E_1 = E_3 = 0.01$, $E_2 = 0.02$. (f). $x = \epsilon = 0.2$, $t = 0.1$, $Rn = 1$, $Gr = 1$, $Qr = 0.3$, $\lambda_1 = 1$, $Br = 0.5$, $Pr = 1$, $Nb = 0.1$, $M = 0.2$, $\beta_1 = \beta_2 = \beta_3 = 0.1$, $E_1 = E_3 = 0.01$, $E_2 = 0.02$. (g). $x = \epsilon = 0.2$, $t = 0.1$, $Rn = 2$, $Gr = 1.5$, $Qr = 0.3$, $\lambda_1 = 1$, $Br = 1.7$, $Nt = 0.1$, $Nb = 1$, $M = 0.2$, $\beta_1 = \beta_2 = \beta_3 = 0.1$, $E_1 = E_3 = 0.01$, $E_2 = 0.02$. (h). $x = \epsilon = 0.2$, $t = 0.1$, $Gr = 1.5$, $Qr = 0.3$, $\lambda_1 = 1$, $Br = 1.7$, $Pr = 1$, $Nt = 3$, $Nb = 2$, $M = 0.2$, $\beta_1 = \beta_2 = \beta_3 = 0.1$, $E_1 = E_3 = 0.01$, $E_2 = 0.02$. (i). $x = \epsilon = 0.2$, $t = 0.1$, $Gr = 1$, $Qr = 1$, $Rn = 1$, $Gr = 1$, $Qr = 0.3$, $\lambda_1 = 1$, $Br = 0.5$, $Pr = 1$, $Nt = Nb = 0.1$, $M = 0.2$, $\beta_1 = \beta_2 = \beta_3 = 0.1$.

doi:10.1371/journal.pone.0148002.g003

viscous dissipation which enhances the temperature. It is reasonable to say that rise in temperature is produced by the stress-reversal process that develops with an increase in β_2 (see Fig 3 (b)). The similar observation for Carreau fluid have been reported by Vajravelu et al. [15]. By increasing Jeffrey nanofluid parameter the temperature profile enhances (see Fig 3(c)). Magnetic force acts as a retarding force and so it slows down the motion of fluid particles. As a result the kinetic energy decreases and thus temperature decreases by increasing Hartman number M (see Fig 3(d)). Here the obtained numerical results are found well matched with the perturbed results by Hayat et al. [7]. Temperature is more for increasing values of Brownian motion parameter Nb because it makes the motion of nanoparticles stronger (see Fig 3(e)). However it decreases for increasing values of thermophoresis parameter Nt (see Fig 3(f)). Since nanoparticles possess strong thermal gradients producing nonlinear dependence of the drift velocity on the applied gradient for large Nt. Thus nonlinear thermophoresis can cause contradictory results between thermophoretic and numerical analysis. That is why the numerical results develops the nonlinear temperature distribution with Nt similar to the study of Hayat et al. [13]. Temperature shows increasing behavior for larger Prandtl number Pr (see Fig 3(g)). It is in view of an increase in specific heat. An increase in thermal radiation parameter Rn decreases the temperature (as noticed from Fig 3(h)). Temperature is the increasing functions

of E_1 and E_2 due to elastance of wall while it decreases for E_3 as E_3 shows oscillatory resistance (see Fig 3(i)).

3.3 Nanoparticle concentration profile

Fig 4 illustrates the influences of various parameters on nanoparticles concentration profile. It is noticed that by increasing values of concentration slip parameter β_3 the nanoparticle concentration decreases (see Fig 4(a)). Fig 4(b) shows that concentration is a decreasing function of Jeffrey nanofluid parameter λ_1. An increasing behavior of nanoparticle concentration is seen with Brownian motion parameter Nb (see Fig 4(c)). Also nanoparticle concentration profile is decreasing function of thermophoresis parameter Nt (see Fig 4(d)). Fig 4(e) depicts that when E_1 and E_2 increased then concentration profile decreases while it increases for E_3.

3.4 Heat transfer coefficient

Fig 5 describes the influence of various emerging parameters on Z. It has been observed that because of successive contraction and relaxation of peristaltic walls the heat transfer coefficient shows oscillatory behavior. For thermal slip parameter β_2 the absolute value of Z decreases (see Fig 5(a)). Heat transfer is an increasing function of Prandtl number Pr (see Fig 5(b)). Also larger radiation parameter Rn enhances the heat transfer coefficient Z (see Fig 5(c)).

4 Concluding remarks

Analysis is performed for the peristaltic flow of Jeffrey nanofluid in a channel with compliant walls partial slip and mixed convection. The major observations are listed below:

- Behavior of λ_1 on velocity and temperature is similar.
- Concentration and temperature have reverse effect for λ_1.
- Grashoff number Gr and local nanoparticle Grashoff number Qr enhance the velocity.

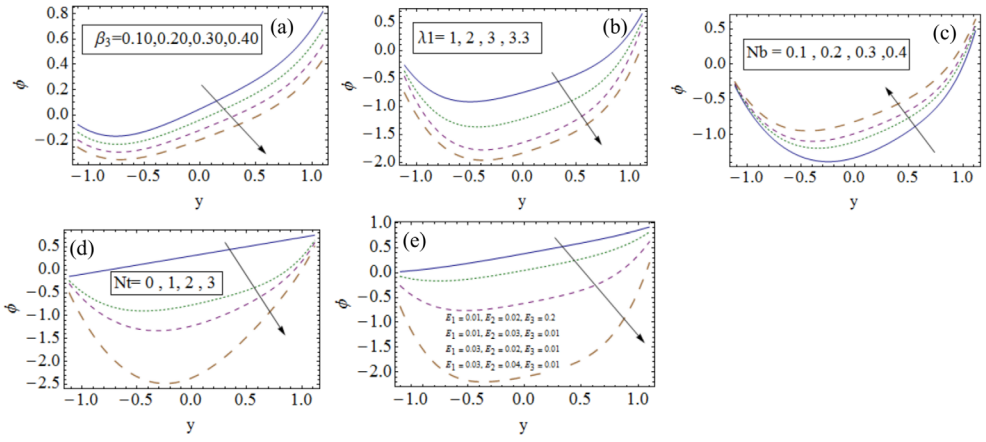

Fig 4. Influences of different parameters on nanoparticle concentration profile when (a). $x = \epsilon = 0.2$, $t = 0.1$, $Gr = 1$, $Qr = 0.3$, $Br = 0.5$, $Nt = Nb = 0.1$, $Pr = 1$, $M = 0.2$, $\lambda_1 = 1$, $Rn = 1$, $\beta_1 = \beta_2 = 0.1$, $E_1 = E_3 = 0.01$, $E_2 = 0.02$. (*b*). $x = \epsilon = 0.2$, $t = 0.1$, $Gr = 0.8$, $Qr = 1$, $Pr = 1$, $Br = 1.7$, $M = 0.2$, $Rn = 1$, $\beta_1 = \beta_2 = \beta_3 = 0.1$, $E_1 = E_3 = 0.01$, $E_2 = 0.02$. (*c*). $x = \epsilon = 0.2$, $t = 0.1$, $Gr = 0.8$, $Qr = 0.3$, $Br = 1.7$, $Nt = 0.1$, $Pr = 1$, $M = 0.2$, $\lambda_1 = 1$, $Rn = 1$, $\beta_1 = \beta_2 = \beta_3 = 0.1$, $E_1 = E_3 = 0.01$, $E_2 = 0.02$. (*d*). $x = \epsilon = 0.2$, $t = 0.1$, $Gr = 1$, $Br = 1.7$, $Qr = 0.3$, $\lambda_1 = 1$, $Rn = 1$, $Nb = 0.3$, $Pr = 1$, $M = 0.2$, $\beta_1 = \beta_2 = \beta_3 = 0.1$, $E_1 = E_3 = 0.01$, $E_2 = 0.02$. (*e*). $x = \epsilon = 0.2$, $t = 0.1$, $\beta_1 = \beta_2 = \beta_3 = 0.1$, $Gr = 1$, $Qr = 0.3$, $Br = 0.5$, $Nt = Nb = 0.1$, $Pr = 1$, $M = 0.2$, $\lambda_1 = 1$, $Rn = 1$, $\beta_1 = \beta_2 = \beta_3 = 0.1$.

doi:10.1371/journal.pone.0148002.g004

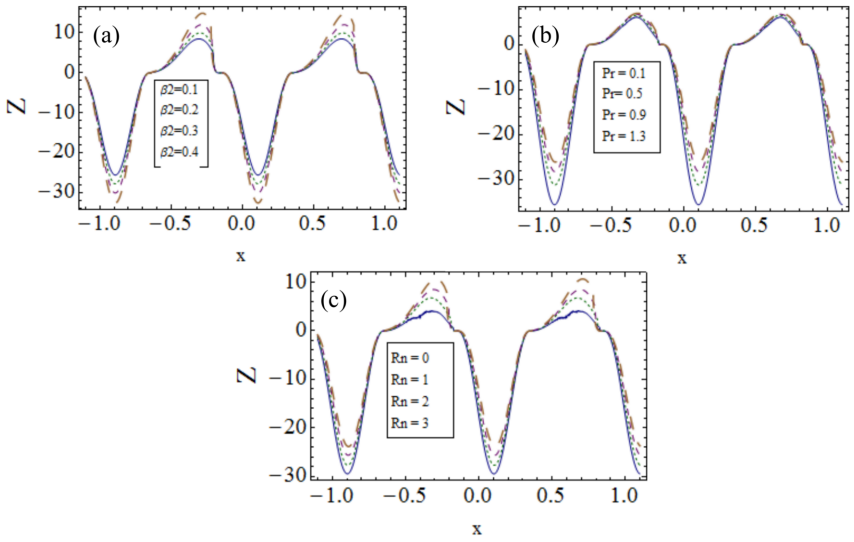

Fig 5. Influences of different parameters on heat transfer coefficient Z(x) when (a). $\epsilon = 0.2$, $t = 0.1$, $Rn = 2$, $Gr = 0.3$, $Qr = 1$, $\lambda_1 = 1$, $Br = 0.5$, $Pr = 1$, $Nt = Nb = 1$, $M = 2$, $\beta_1 = \beta_3 = 0.1$, $E_1 = 0.1$, $E_3 = 0.01$, $E_2 = 0.2$. (b). $\epsilon = 0.2$, $t = 0.1$, $\lambda_1 = 1$, $Rn = 2$, $Gr = 0.3$, $Qr = 1$, $Nt = Nb = 1$, $M = 2$, $\beta_1 = \beta_2 = \beta_3 = 0.1$, $E_1 = 0.1$, $E_3 = 0.01$, $E_2 = 0.2$. (c). $\epsilon = 0.2$, $t = 0.1$, $Gr = 0.3$, $Qr = 1$, $Br = 0.4$, $Nt = Nb = 0.1$, $M = 2$, $\beta_1 = \beta_2 = \beta_3 = 0.1$, $E_1 = 0.1$, $E_3 = 0.01$, $E_2 = 0.2$.

doi:10.1371/journal.pone.0148002.g005

- Qualitatively the radiation *Rn* and thermophoresis *Nt* parameters have same effects on temperature.
- Brownian motion parameter enhances the temperature.
- Effects of E_1 and E_2 on velocity are similar. However the impact of E_3 on velocity is opposite to that of E_1 and E_2.
- Behaviors of β_1 on velocity and β_2 on temperature are similar. However concentration decreases upon increasing slip parameter β_3.
- Hartman number *M* reduces the temperature and velocity.
- Both temperature and heat transfer coefficient are increased for Prandtl number Pr.
- Concentration profile is decreasing function of E_1 and E_2. However the role of E_3 on concentration is reverse to that of E_1 and E_2.

Author Contributions

Conceived and designed the experiments: TH MS AT AA. Performed the experiments: TH MS AT AA. Analyzed the data: TH MS AT AA. Contributed reagents/materials/analysis tools: TH MS AT AA. Wrote the paper: TH MS AT AA.

References

1. T. W. Latham, Fluid motion in peristaltic pumps, M S. Thesis, MIT, Cambridge, MA, 1966.
2. Shapiro A. H., Jaffrin M. Y. and Weinberg S. L., Peristaltic pumping with long wavelengths at low Reynolds number, J. Fluid Mech, 37 (1969) 799–825. doi: 10.1017/S0022112069000899
3. Hayat T., Yasmin H. and Al-Yami M., Soret and Dufour effects in peristaltic transport of physiological fluids with chemical reaction, A mathematical analysis, Comp. Fluids, 89 (2014) 242–253. doi: 10.1016/j.compfluid.2013.10.038

4. Mekheimer Kh. S., Abd elmabond Y. and Abdellateef A. I., Peristaltic transport through eccentric cylinders, Mathematical model, Appl. Bio. Biomech, 10 (2013) 19–27. doi: 10.1155/2013/902097
5. Tripathi D. and Beg O. A., A study on peristaltic flow of nanofluids: Application in drug delivery systems, Int. J. Heat Mass Transf. 70 (2014) 61–70. doi: 10.1016/j.ijheatmasstransfer.2013.10.044
6. Hayat T., Abbasi F. M., Alsaedi A., and Alsaadi F., Hall and Ohmic Heating Effects on the Peristaltic transport of a Carreau–Yasuda fluid in an asymmetric channel, ZNA, 69 (2014) 43–51.
7. Hayat T., Tanveer A., Yasmin H. and Alsaedi A., Homogeneous-Heterogeneous Reactions in Peristaltic flow with convective conditions, PLOS ONE, 9 (2014) e113851. doi: 10.1371/journal.pone.0113851 PMID: 25460608
8. Abbasi F. M., Hayat T. and Ahmad B., Peristaltic transport of copper–water nanofluid saturating porous medium, Physica E:, 67 (2015) 47–53. doi: 10.1016/j.physe.2014.11.002
9. Hayat T., Abbasi F. M. and Alsaedi F., Hydromagnetic peristaltic transport of water-based nanofluids with slip effects through an asymmetric channel, Int. J. Mode. Phy., 29 (2015) (17 pages).
10. Ellahi R., Bhatti M. M. and Vafai K., Effects of heat and mass transfer on peristaltic flow in a non-uniform rectangular duct, Int. J. Heat Mass Transf., 71 (2014) 706–719. doi: 10.1016/j.ijheatmasstransfer.2013.12.038
11. Hina S., Hayat T., Mustafa M. and Alsaedi A., Peristaltic transport of pseudoplastic fluid in a curved channel with wall properties and slip conditions, Int. J. Biomath., 7 (2014) (16 pages). doi: 10.1142/S1793524514500156
12. Gad N. S., Effects of Hall currents on peristaltic transport with compliant walls, Appl. Math. Comput., 235 (2014) 546–554. doi: 10.1016/j.amc.2014.02.081
13. Hayat T., Nisar Z., Ahmad B. and Yasmin H., Simultaneous effects of slip and wall properties on MHD peristaltic motion of nanofluid with Joule heating, J. Magn. Magn. Mater., 395 (2015) 48–58.
14. Ebaid A. and Aly E. H., Exact analytical solution of the peristaltic nanofluids flow in an asymmetric channel with flexible walls and slip condition, Compu. Math. Meth. Med., 2013 (2013) (8 pages). doi: 10.1155/2013/825376
15. Vajravelu K., Sreenadh S. and Saravana R., Combined influence of velocity slip, temperature and concentration jump conditions on MHD peristaltic transport of a Carreau fluid in a non-uniform channel, Appl. Math. Comput., 225 (2013) 656–676. doi: 10.1016/j.amc.2013.10.014
16. Hayat T., Rafiq M., Alsaedi A. and Ahmad B., Radiative and Joule heating effects on peristaltic transport of dusty fluid in a channel with wall properties, Eur. Phys. J. Plus, 129 (2014) 225. doi: 10.1140/epjp/i2014-14225-9
17. Nadeem S. and Akbar N. S., Influence of radially varying MHD on the peristaltic flow in an annulus with heat and mass transfer, J. Taiwan Inst. Chem. Eng., 41 (2010) 286–294. doi: 10.1016/j.jtice.2009.11.004
18. Ellahi R. and Hussain F., Simultaneous effects of MHD and partial slip on peristaltic flow of Jeffrey fluid in a rectangular duct, J. Magn. Magn. Mater., 393 (2015) 284–292. doi: 10.1016/j.jmmm.2015.05.071
19. Ali N., Javed K., Sajid M. and Beg O. A., Numerical simulation of peristaltic flow of a biorheological fluid with shear dependent viscosity in a curved channel, Comp. Meth. Biomech. Biomed., 59 (2015) 1–14.
20. Sheikholeslami M., Bandpy M. G., Ellahi R. and Zeeshan A., Simulation of MHD CuO–water nanofluid flow and convective heat transfer considering Lorents forces, J. Magn. Magn. Mater., 369 (2014) 69–80. doi: 10.1016/j.jmmm.2014.06.017
21. Abbasi F. M., Hayat T. and Alsaedi A., Effects of inclined magnetic field and Joule heating in mixed convective peristaltic transport of non-Newtonian fluids, Bull. Polish. Acad. Sci. Tech. Sci., 63 (2015).
22. Mustafa M., Abbasbandy S., Hina S. and Hayat T., Numerical investigation on mixed convection peristaltic flow of fourth grade fluid with Soret and Dufour effects, J. Taiwan. Inst. Chem. Eng., 45 (2014) 308–316. doi: 10.1016/j.jtice.2013.07.010
23. Hayat T., Abbasi F. M., Al-Yami M. and Monaquel S., Slip and Joule heating effects in mixed convection peristaltic transport of nanofluid with Soret and Dufour effects, J. Mol. Liquids, 194 (2014) 93–99. doi: 10.1016/j.molliq.2014.01.021
24. Srinivas S. and Muthuraj R., Effects of chemical reaction and space porosity on MHD mixed convective flow in a vertical asymmetric channel with peristalsis, Math. Computer Modeling, 54 (5–6) (2011) 1213–1227. doi: 10.1016/j.mcm.2011.03.032
25. Srinivas S., Gayathri R. and Kothandapani M., Mixed convective heat and mass transfer in an asymmetric channel with peristalsis, Comm. Nonlinear Sci. Num. Simulation, 16 (2011) 1845–186. doi: 10.1016/j.cnsns.2010.08.004